

Characterization of Gaseous and Particle Emissions of a Direct Injection Hydrogen Engine at Various Operating Conditions

Downloaded from: https://research.chalmers.se, 2026-11-14 18:29 UTC

Citation for the original published paper (version of record):

Berg, V., Koopmans, L., Sjöblom, J. et al (2023). Characterization of Gaseous and Particle Emissions of a Direct Injection Hydrogen Engine at
Various Operating Conditions. SAE Technical Papers. http://dx.doi.org/10.4271/2023-32-0042

N.B. When citing this work, cite the original published paper.

research.chalmers.se offers the possibility of retrieving research publications produced at Chalmers University of Technology. It covers all kind of research output: articles, dissertations, conference papers, reports etc. since 2004. research.chalmers.se is administrated and maintained by Chalmers Library

(article starts on next page)

Downloaded from SAE International by Chalmers University of Technology, Friday, November 06, 2026

2023-32-0042 Published 29 Sep 2023

Characterization of Gaseous and Particle Emissions of a Direct Injection Hydrogen Engine at Various Operating Conditions

Victor Berg, Lucien Koopmans, Jonas Sjöblom, and Petter Dahlander Chalmers University of Technology

Citation: Berg, V., Koopmans, L., Sjöblom, J., and Dahlander, P., "Characterization of Gaseous and Particle Emissions of a Direct Injection Hydrogen Engine at Various Operating Conditions," *SAE Int. J. Advances & Curr. Prac. in Mobility* 6(3):1746-1757, 2024, doi:10.4271/2023-32-0042.

This article was presented at the JSAE/SAE Powertrains, Energy and Lubricants International Meeting, August 29-September 1, 2023.

Abstract

This paper investigates the gaseous and particulate emissions of a hydrogen powered direct injection spark ignition engine. Experiments were performed over different engine speeds and loads and with varying air- fuel ratio, start of injection and intake manifold pressure. An IAG FTIR system was used to detect and measure a variety of gaseous emissions, which include standard emissions such as NOX and unburned hydrocarbons as well as some non-standard emissions such as formaldehyde, formic acid, and ammonia. The particle number concentration and size distribution were measured using a DMS 500 fast particle analyzer from Cambustion. Particle composition was investigated using ICP analysis as well as a Sunset OC/EC analyzer to determine the soot content and the presence of any unburned engine oil. The results show that NO_X emissions range between 0.1 g/kWh for a λ of 2.5 and 10 g/kWh λ of 1.5. The highest particle concentration was found for low loads and low intake pressures, with peaks values as high as $5*10^8$ n/cc. ICP analysis confirmed that the particles contained traces of engine oil, while the OC/EC analysis showed that 99% of particle matter collected on filters was organic carbon, and <1% soot. The emissions of N_2O as well as several other species measured with FTIR was found to be in the single ppm range, and thus not significant.

Introduction

The increased focus on greenhouse gas emissions has caused a renewed interest in renewable fuels, as efficiency improvements alone are incapable of reducing the emissions to harmless levels while running on fossil fuels. Related to this, the transport sector has a unique set of challenges, most notably the energy density of the energy carrier (range and air-fuel mixing time with direct injected systems) and the power density of the powertrain (required air-fuel-ratio and partial pressure of the gaseous fuel) and any after-treatment system needed to reduce emissions to harmless levels.

Hydrogen is a potential fuel for future transport solutions. Hydrogen is the simplest possible form of electro fuel that can be produced and contains no carbon. It has therefore the potential to reach climate goals if the hydrogen is produced from renewable sources [1].

Hydrogen can be used to fuel either a fuel cell or a combustion engine. Both solutions have their relative benefits and drawbacks. For fuels cells, drawbacks involve cost, complexity, volumetric power density of the system and questions regarding longevity. The benefits of fuel cells are zero tank to wheel (TTW) greenhouse gas emissions and relatively high efficiency [2]. The benefits of an internal combustion engine operated on hydrogen are zero TTW CO_2 GHG emissions, a relatively high power-density, cheap and robust, and good efficiency at high power. This article focuses on one of the drawbacks that needs to be overcome for a hydrogen combustion engine to be viable, namely local air-quality emissions.

The volumetric power density of a hydrogen combustion engine is typically much lower than a comparable spark ignition engine operated on gasoline. This is mostly caused by the low density of hydrogen, hence a significant volume in the cylinder will be occupied by fuel. If injected early this will displace air going into the cylinder thus reducing power density further [3]. Direct hydrogen injection in internal combustion engines has seen renewed interest as it can help alleviate some of these drawbacks. Direct injection (DI) has the potential to let the start of injection of fuel occur after the intake valve has closed [3, 4] something that should in theory eliminate the risk of backfiring completely and help increase power density since it avoids air-displacement. DI has drawbacks however, as the hydrogen injected in the cylinder can hit the cylinder wall, which can increase the particle emissions [5]. Using DI to inject hydrogen after the intake valve closes is attractive for power density and to reduce pumping work, but can lead to inhomogeneous mixing and increased NOX emissions [4, 6, 7].

© 2023 The Author(s); Published by SAE International. This Open Access article is published under the terms of the Creative Commons Attribution License (http://creativecommons.org/licenses/by/4.0/), which permits distribution, and reproduction in any medium, provided that the original author(s) and the source are credited.

Downloaded from SAE International by Chalmers University of Technology, Friday, November 06, 2026

The emissions of a hydrogen-fueled internal combustion engine mainly consist of nitrogen oxides (NOX) and particulates. NOX emissions for hydrogen engines can be reduced to very low levels by running the engine at very lean conditions [3, 4, 8, 9, 10]. Very lean operation poses challenges for the power density, as more air needs to be ingested, and lean operation at high loads while maintaining power density requires significant boosting levels with the risk of auto-ignition and engine knock and exceeding the maximum cylinder pressure.

With new emissions regulations, such as the new EURO 7 regulation [11], a number of new species are introduced in the legislation, and it is essential to investigate what the emission levels of these species are.

Previous experiments conducted have also shown that even though a hydrogen engine should produce no particles from the combustion of the fuel, particle emissions are significant [12]. It was concluded that the only source of particle emissions was the engine oil, and tests with different oils seemed to confirm this. The engine out particle emissions in the sub 30 nm range of a hydrogen fueled engine closely resembles the particle emissions of the same engine fueled with gasoline or methane. Hydrogen does however give lower emission of larger particles. The source of particles of the smaller sizes range was engine oil, as demonstrated by the independence of the fuel used [12].

The same study on fuel independent particle emissions from an engine found that particle emission from a DI SI engine operated on hydrogen gave high emissions of very fine particles, i.e., <10 nm, but produced fewer large particles than on gasoline operation. Peak dN/dlog(Dp) around 1e8 n/cc. Inlet air particles were measured and found to be negligible compared to the levels found in the exhaust. Particle emissions in numbers per unit volume in the lower size range (3-30 nm) matched those of gasoline, while less agglomeration particles were found [12].

An investigation into the effects of different lubricating oils on the particle emissions from an engine operated on a hydrogen rich reformate [13], showed significantly higher emission from an engine operated on a hydrogen rich reformate compared to gasoline regardless of which of the engine oil were used. The Author(s) also found from inductively coupled plasma analysis (ICP) that the particles from the reformate fuel contained higher quantities of trace elements from the oil, which points to increased oil involvement in the combustion process. An explanation proposed by the Author(s) was that the high speed of the high-pressure hydrogen jet at the point where it impinges on the cylinder wall would remove oil from the cylinder wall. The turbulent jet could also entrain adjacent oil vapours into the jet, which in turn could increase emissions of particles. Thawko et al. operated a DI SI engine on hydrogen rich reformate produced by methanol steam reforming. The fuel was 75% H2 and 25% CO2 by volume. The particle emissions was measured with an engine exhaust particle sizer (EEPS), using a hose heated to 300 °C to avoid volatiles [5]. Particle numbers (PN) reported was up to $4*10^6$ at a size of 10 nm for an engine load of 4.5 bar indicated mean effective pressure (IMEPnet) at 3000 rpm with a small secondary peak in the size distribution at 80 to 100 nm for DI operation. Operation with port fuel injection (PFI) was shown to produce less particles in the same study. The DI engine when fuelled with steam methane reforming products was found to produce higher particle numbers than the same engine operated on gasoline, especially in the lower size range. The larger particles contribute most to the particle mass (PM). The total PM concentration was shown to be 42% higher compared to DI gasoline operation.

Most of the research performed so far has focused on a single engine operating point, reporting the emissions of common legislated species. This research focuses on investigating the total emissions from a direct injected hydrogen engine over a variety of operating points and investigating parameters affecting these emissions as well as to investigate the origin of the particulate emissions further.

Methods

Engine Setup

A single cylinder, direct injected spark ignited engine was used for all experimental work described in this paper. The engine geometry is from a typical state-of- the-art light duty spark ignited gasoline engine. Thus, the engine is slightly undersquare and has 4 valves per cylinder. The only modifications made to the cylinder head was that the liquid fuel injector was replaced with a prototype gas injector from GDTech and the spark plug was exchanged to a platina-free one to minimize pre- ignition. Some of the relevant engine parameters are displayed in Table 1.

The engine's crankcase ventilation system was externally force vented, and not fed back to the intake to reduce the risk of buildup of hydrogen in the crankcase. The forced ventilation was used to increase the air flow to the crankcase, thus diluting the hydrogen in the blow- by gases. As the higher loads in the experiments necessitated intake pressures above atmospheric, there would be no point with pressure lower than the crankcase to vent the gases to, which required the crankcase to be vented to the low pressure created by the test cell's exhaust fan.

The hydrogen injection pressure was controlled by a mechanical pressure regulator. The injector was fed through a single pipe, without any buffer reservoir. The volume of the pipe from the pressure regulator to the injector was large enough to avoid significant pressure drop during injection.

TABLE 1 Engine specifications for the single cylinder engine.

Displacement volume (dm^3)	0.475
Bore (mm)	90
Stroke (mm)	82
Conrod length (mm)	139.5
Compression ratio (CR) (-)	10:1
Intake valve opening (IVO) (°aTDC)	356
Intake valve closing (IVC) (°aTDC)	-142
Exhaust valve opening (EVO) (°aTDC)	145
Exhaust valve closing (EVC) (°aTDC)	357

© The Author(s)

Downloaded from SAE International by Chalmers University of Technology, Friday, November 06, 2026

This was verified with a fast pressure sensor mounted in the hydrogen pipe just upstream of the injector.

The injector was a ten-hole, inward opening solenoid type, where 9 of the orifices were arranged in a cone around the central vertically oriented middle orifice. The mass flow rate of the injector was found to be highly dependent on the injection pressure, hence the injection pressure had to be adjusted to reach the target load.

The operating pressures of the injector were in the range of 10 to 50 bar.

Measurement Setup

An IAG Fourier-transfer infrared system (FTIR) was used to measure NO, NO_2 as well as several currently non- regulated emissions that are included in the current EURO 7 proposal, such as NH_3, N_2O and formaldehyde (HCHO) [11]. The FTIR was also used to measure the water content as well as the CO and CO2 emissions.

Since the FTIR cannot measure any homonuclear diatomic gases, such as O_2 and H_2, additional measurement equipment was used. The equipment used to measure emissions in addition the FTIR are summarized in Table 2.

A J.U.M. VE7 flame ionization detector (FID) analyzer was used to measure total hydrocarbons (THC) in the exhaust, as the FTIR is limited to lower hydrocarbons emissions and has a slight cross sensitivity to water that affects the measurements. Excess air-, λ, was used for engine control purposes and was measured with a Horiba Mexa-110.

Hydrogen emissions in the exhaust stream were measured by a NeoHysens NEO951A sensor. The sensor can withstand temperatures up to 400 °C and pressures up to 1.2 bar absolute. To keep the temperature and pressure within the acceptable range, the sensor was mounted downstream of the exhaust buffer tank and the back-pressure valve. In total the distance from the exhaust port was several meters, which would allow the gases too cool down from the temperature in the exhaust port, which was less than 550 °C for the operating points considered. The sensor was originally planned to be used to estimate combustion efficiency and as a safety feature. The hydrogen emissions were however within the 0.5% measurement error; hence the results were omitted from this paper. The sensor was also used to verify that the hydrogen concentration in the crankcase gases was below the flammability limit, by running a sample selection of load points with the sensor mounted in the crankcase ventilation pipe.

TABLE 2 Emission measurement devices and accuracies for the additional measurement devices.

Species	Instrument	Range	Unit	Error
PN	Cambustion DMS500 MkII	0-300	nm	± 5.00 %
		300-1000	nm	± 10 %
THC	J.U.M. VE7	0-1000	ppm	± 1.00 %
H_2	NeoHysens NEO951A	0-5	%	± 0.50 %
λ	Horiba Mexa-110	0.5-2.5	λ	± 0.70 %

© The Author(s)

Particle numbers and size distributions were measured with a Cambustion DMS 500 fast particle analyzer, without any catalytic stripper. The DMS was connected to the exhaust runner, upstream of the exhaust buffer tank to reduce the possible contamination from old deposits in the exhaust system and maintain exhaust temperatures to avoid condensation. The location of the sampling points meant that the inlet to the DMS would be subject to pressures above atmospheric, as it is upstream of the throttle used to create back pressure at higher loads when boost pressure is simulated. Washers with orifices of different sizes can be installed in the DMS to maintain the correct flow rate at different pressures, but this requires that the engine is shut off each time the washer needs to be changed. To reduce the exhaust pressure to suitable levels for the DMS regardless of exhaust pressure, an AVL pressure reducer unit was mounted between the DMS intake cyclone and the exhaust pipe. This reduced the pressure to atmospheric levels, which enabled the DMS to maintain the desired sampling flow.

Particles were also collected on filters, by pulling exhaust gases through a filter element at a rate of 10 l/min using a vacuum pump. The engine was operated at the lowest load point of 2.5 bar IMEP and 1000 rpm, marked in green in Figure 2, which was found from preliminary tests to produce a large quantity of particle emissions. While the DMS showed that the engine produced significant particle numbers, the particles are in general very small with a peak somewhere between 10 and 30 nm. Thus, the expected total particle mass is low, which required long sampling times.

Sampling for inductively coupled plasma (ICP) analysis took place over 10, 30 and 85 minutes, respectively, on 3 Teflon filters. The load point was the lowest load at the lowest speed from the engine mapping experimental campaign, indicated in green in Figure 2. Different sampling times was used as the possible concentration of metal particles was unknown, and a good range for the instrument was desired. Further, an increase in sampling time would allow a proportional increase in the collected particles. The total mass of particles was calculated assuming spherical particles with a density of 1000 kg per m^3, as the composition of particles was unknown at this point. The particle mass on the filters reported in the result section is thus approximate.

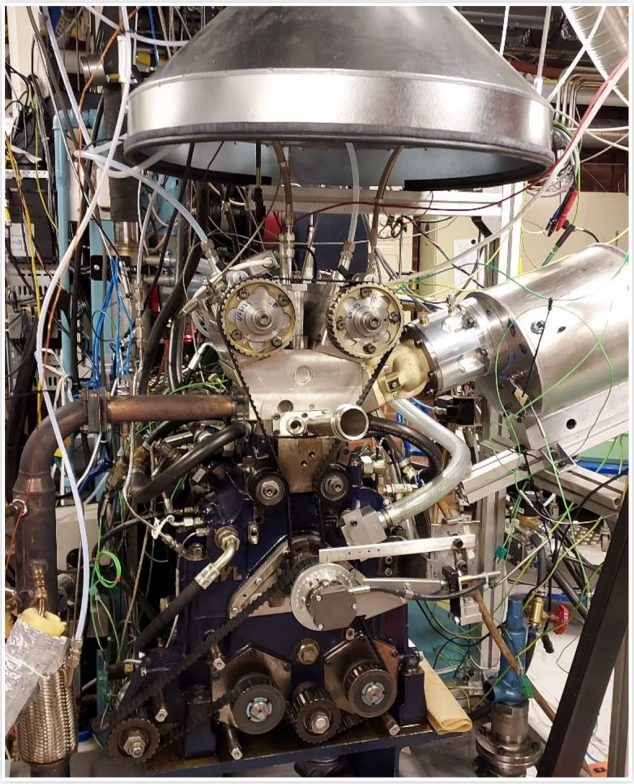
For the Sunset organic carbon/elemental carbon (OC/EC) analysis, 2 filters were used. The Sunset OC/EC analyzer works by heating samples and measuring the emission of hydrocarbons with a FID in both in helium to capture the organic carbon compounds that evaporate, and in the presence of oxygen to detect elemental carbon. To make sure that the results was not affected by Teflon vapors or breakdown as the samples were heated, the filters used were made from quartz.

Sampling for the first quartz filter was done for 10 minutes for conditions from the lowest load and speed in the engine map at an intake pressure of 0.7 bar. For the second quartz filter, the sampling was repeated, but with the intake pressure increased to 0.8 bar for a time of 30 minutes.

The test setup of the engine is shown in Figure 1. To the left is the exhaust, with the sampling sections for the measurement instruments. The hood above the engine is to capture any hydrogen leakage and is connected to an external fan.

Downloaded from SAE International by Chalmers University of Technology, Friday, November 06, 2026

FIGURE 1 The single cylinder engine used in the experiments.



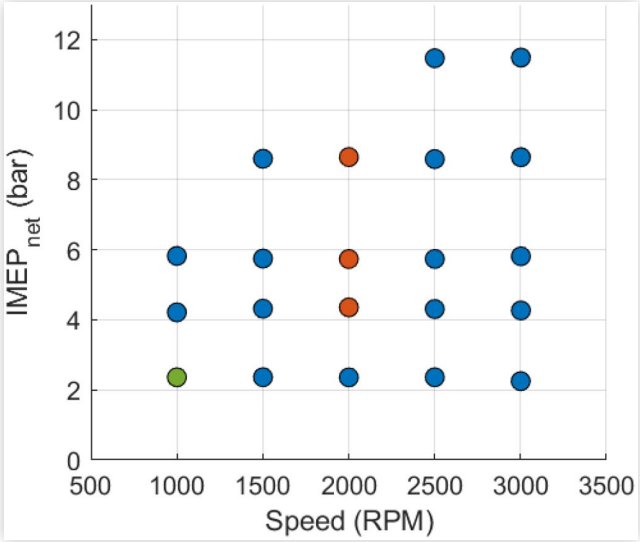
© The Author(s)

Test procedure

Engine map The baseline engine map consisted of engine speeds in a range from 1000 to 3000 rpm. The engine was operated on neat hydrogen at a λ of 2 from a load of 2.5 bar net indicated mean effective pressure (IMEPnet) up to the maximum possible. To achieve higher loads, the intake pressure was increased by an external compressor. To keep operation closer to realistic, turbocharged, conditions, the exhaust back-pressure was increased to the same level as the intake pressure with a throttling valve in the exhaust. For engine speeds below 2500 rpm, the maximum load was limited by the maximum obtainable backpressure in the exhaust, while the load at higher speeds was limited by the maximum opening duration of the hydrogen injector and the maximum allowed injection pressure of 50 bar. For all points, the baseline ignition timing was adjusted to keep 50% mass fraction burned at 8° aTDC, as this was found to be maximum brake torque (MBT) timing in methane operation [14]. The points run in the tests are illustrated in Figure 2.

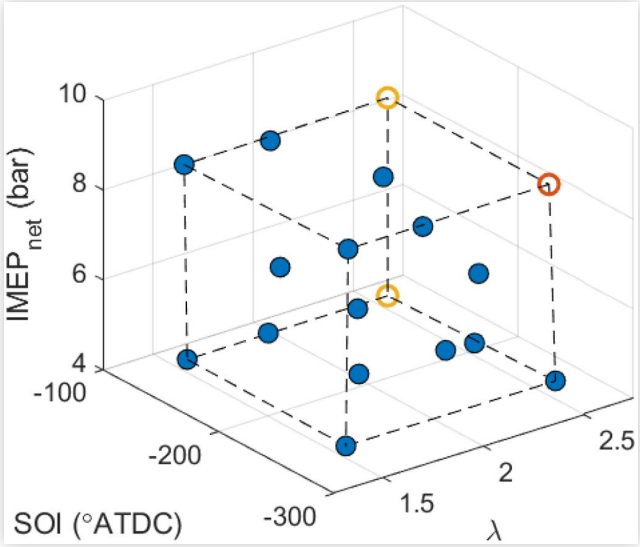
Design of Experiments While the baseline map would give insight into the influence of load and speed at fixed λ of 2, the influence of start of injection and excess air ratio for different loads were investigated in a second round of experiments. A face-centered cubic design of experiments (DoE) approach was used to also investigate any combined effects. This investigation was conducted at a fixed speed of 2000 rpm. The test points used are shown in Figure 3

FIGURE 2 Operating points for the baseline engine map. The points marked in red were also included in the DoE experiments, while the lower left point marked in green shows where particle sampling took place.



© The Author(s)

FIGURE 3 DoE parameters used. Points that could be run on the single cylinder engine are marked in blue.



© The Author(s)

The ability to run the test points at 9 bar IMEP and a λ of 2.5, marked by the red circle in Figure 3, was limited by the pressure that the back pressure valve could provide at lower exhaust flows, which was not enough to match the intake pressure required to reach the target load and air fuel ratio. The points marked by the yellow circles are points where a combination of late SOI at -130° aTDC and very lean conditions at λ = 2.5 led to poor combustion stability. At these points, no measurements could be collected, as the unburnt hydrogen from frequent misfires combusted in the engine's exhaust system. Here the limited time from start of injection to the ignition was presumably not long enough to mix the

Downloaded from SAE International by Chalmers University of Technology, Friday, November 06, 2026

air and hydrogen sufficiently when combined with the higher ignition energy and lower flame speed of very lean mixtures.

Results and Discussion

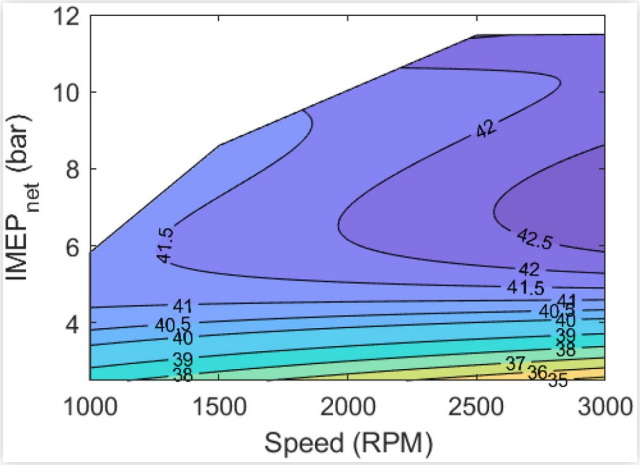
Efficiency

The indicated efficiency shows the highest values for the loads higher than 6 bar IMEPnet, increasing slightly as speed increases, while the lowest efficiencies are found at low load and high speed, see Figure 4. The main cause for the lower efficiencies at those points are the pumping losses. They increase at low loads, during throttled operation, which was required to maintain λ = 2. The pumping losses also increase slightly with increased engine speed, which can explain why efficiencies drop further as the engine sped increased at low loads. Compared to a similar engine run on methane or gasoline, lean operation at lambda 2 limited the throttling losses, and an indicated efficiency could be maintained at over 35 % for the whole investigated load range.

The results from the DoE also showed that for a given load the efficiency increased with leaner combustion. Eliminating throttling losses for the 4.5 bar IMEP case by increasing the excess air ratio increases efficiency and is partly responsible for the higher efficiency. A weaker trend of decreasing efficiency with late SOI can also be seen for this case, indicated by the slightly lower efficiency in the bottom right corner in plot c) in Figure 5, and could be related to the increased throttling losses incurred when the hydrogen is injected closer to IVC. The late injection causes hydrogen to displace less air, and more throttling is required to maintain λ at 2. The efficiency for the three different loads included in the DoE are shown in Figure 5.

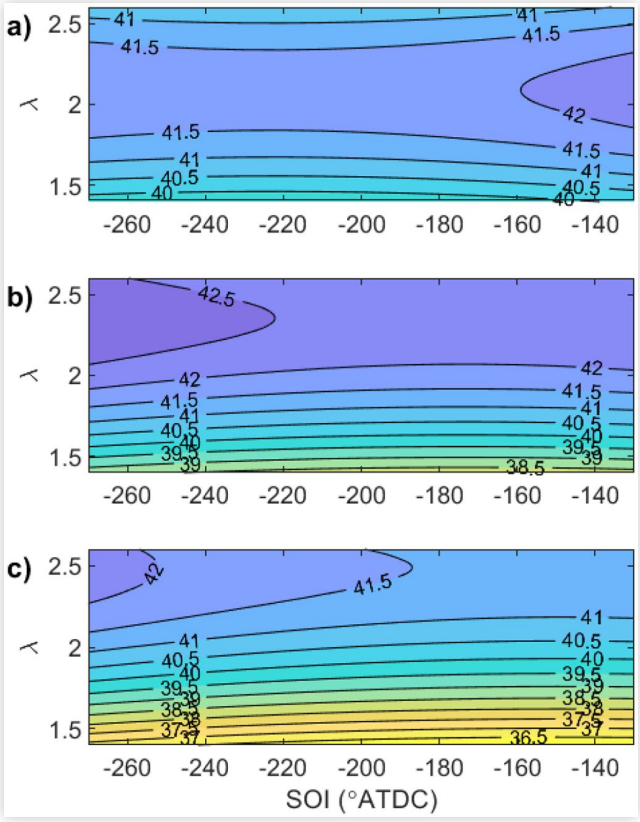
For higher loads, the impact of different injection timings is less significant, and the impact of A/F is the most important. The pumping losses should not be the cause for the drop in efficiency, as the intake pressure and exhaust back pressure was kept at the same level for these loads. The case is most likely the heat losses in the cylinder decreases for lean

FIGURE 4 Indicated efficiency (%) for the load map.



© The Author(s)

FIGURE 5 Indicated efficiency (%) from the DoE for three loads: a) 9 bar IMEPnet, b) 6 bar IMEPnet and c) 4.5 bar $IMEP_{net}$.



© The Author(s)

operation, as the peak cylinder temperatures depends strongly on λ. In general, the efficiency's dependence on λ diminishes at higher loads.

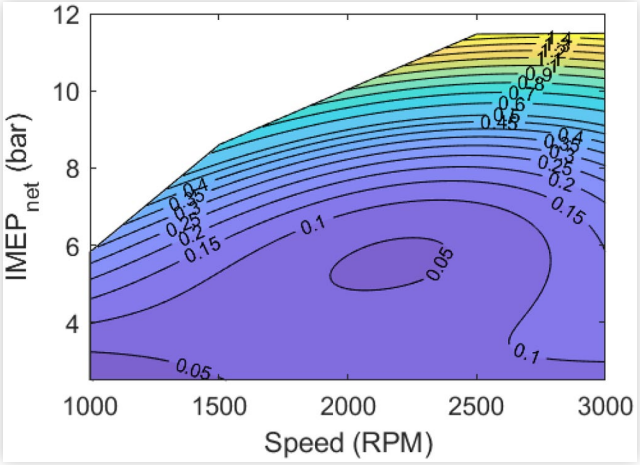
NOx Emissions

For all but the lowest load points in the engine map, NO contributed the most to the total NOX emissions. The baseline lambda of 2 was chosen for the mapping as it appeared to provide a good compromise between maximum load, efficiency, and NOX emissions. Hence, the engine out indicated specific emissions are relatively low, but they exceed 1 g/kWh at the highest loads and engine speeds, which not only exceeds the upcoming EURO 7 [11] but also the older EURO VI [15] legislation for brake emissions and for loads that are lower than those that are normally reached in current heavy-duty Spark ignition (SI) and compression ignition (CI) engines [16]. For most points in the engine map the emissions exceeded those of the proposed EURO 7 legislation, which limits NOX emissions for the warm cycle to 90 mg/kWh. An exhaust after-treatment system would thus be necessary for on-road applications. The emissions over the engine map are shown in Figure 6.

The influence of the λ ratio on the NOX emissions of an SI engine have been studied extensively, in numerous studies on emission reductions and lean burn engine concepts [3, 4, 8, 9, 10]. A hydrogen SI engine follows these trends, which the

Downloaded from SAE International by Chalmers University of Technology, Friday, November 06, 2026

FIGURE 6 Indicated specific NOX emissions (g/kWh) over the engine map



© The Author(s)

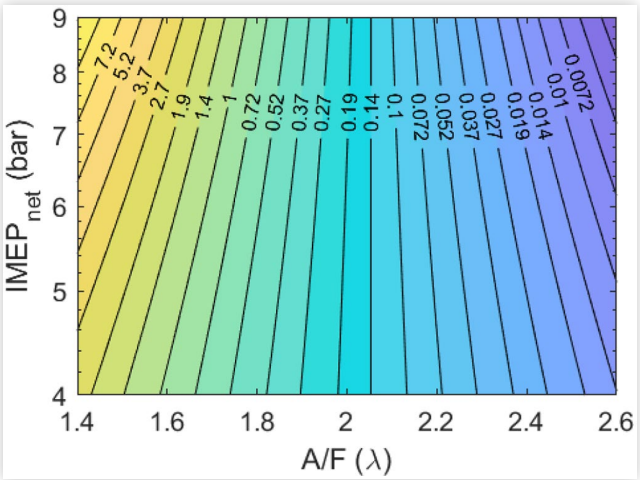
result from the DoE confirms. The main advantage of hydrogen compared to other fuels in this regard is the wide flammability limit, that enabled operation at higher excess air ratios. The increased emissions are most likely due to the increased burn rate and the higher adiabatic flame temperatures of richer flames. In Figure 7, the indicated specific NOX emissions are shown for the baseline combustion phasing. The emissions increase slightly with load and for late SOI, but the main influence is the A/F ratio. Extrapolation of the peak emissions of ~10 g/kWh are found for SOI at -130 °aTDC at a net IMEP of 9 at $\lambda = 1.5$.

The results illustrated in Figure 7 do not consider the effects of combustion phasing. All load points included were run at different in timings to achieve combustion phasing in a range around the assumed MBT phasing of 8°aTDC. With variations in combustion phasing, there is considerable variations in NOX emissions for a given λ, and the A/F ratio alone is not enough to predict the outcome, as seen in the scatter plot in Figure 8.

The NOX emissions show an exponential increase for lower A/F ratios, but also with decreased burn duration from MFB 10 to MFB 90, regardless of A/F. A simple line was fitted to the data, of the form $\log(Y) = \beta_0 + \beta_1 x_1$. A line was chosen as the large spread in the data was seen and the R^2 of the model would only improve marginally if a polynomial of higher order was used instead. For models fitted to the logarithmic NOX emissions including only the variable from the x-axis shown in Figure 8, the lambda-based model showed a slightly better fit than the model based on MFB 10-90, with an R^2 value of 0.646 versus 0.613, respectively. The low R^2 values could be improved by introducing mor variables into the linear model. While the deviations from the line fitted to the data in the top graph in Figure 8 can only be partially explained with the effects of e.g., combustion phasing, the deviations in the measurement values in the bottom graph showed a strong dependence on the net load of the engine. Results from the DoE experiments confirm that load has little influence on the burn duration with an R^2 <0.05 for the best fitting linear model that could be constructed, meaning that the two variables are largely independent. The burn duration and load can thus be used to predict NOX emissions to a relatively high accuracy with a simple linear fit to the logarithm of the indicated specific NOX emissions while using only two variables, as shown in Figure 9.

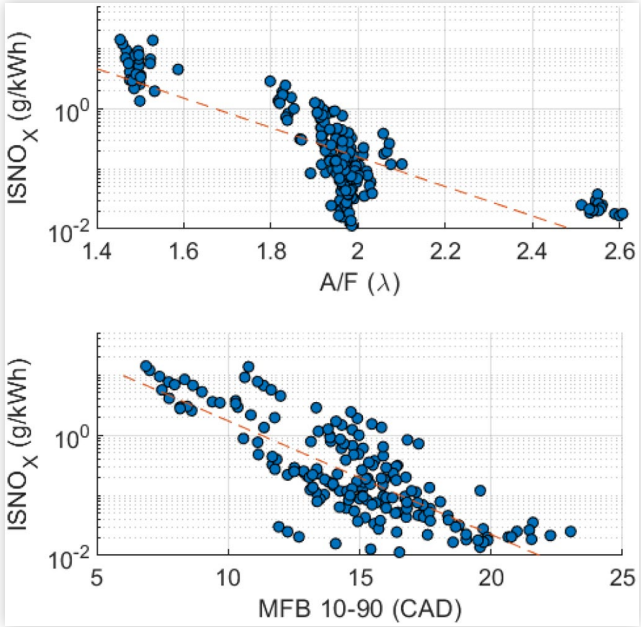
The R^2 value for this model is 0.86, which was the highest R^2 value that could be obtained for a such a simple model, of the form $\log(Y) = \beta_0 + \beta_1 x_1 + \beta_2 x_2$. If this assumption holds, it will mean that an alternative approach to reduce the NOX emissions of a lean burn hydrogen engine would be to try to slow down the combustion, increasing the burn duration,

FIGURE 7 Indicated specific NO_X emissions (g/kWh) for the data points included in the DoE, for SOI at -200 °aTDC. The influence of SOI on the NO_X emissions was found to be small compared to the influence of λ and IMEP



© The Author(s)

FIGURE 8 Indicated specific NO_X emissions (g/kWh) as a function of A/F ratio (top) and MFB 10-90 (bottom). The best available line fit trough the measured data points are shown in red.



© The Author(s)

Downloaded from SAE International by Chalmers University of Technology, Friday, November 06, 2026

FIGURE 9 Indicated specific NOx emissions, modeled (grid) and measured (dots). The red dotted lines show the distance from the modeled surface to the measured data.

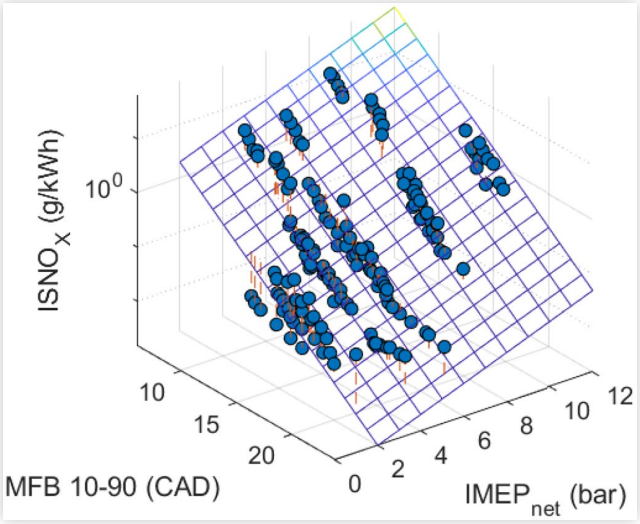
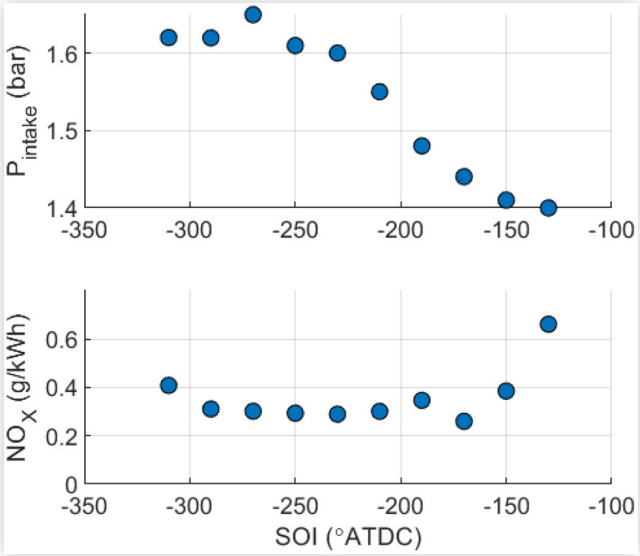


FIGURE 10 Intake pressure required for λ=2 and NOX emissions vs SOI. for a load of 9 bar at 2000 rpm.



either by delaying the spark timing or other means. Water injection, for example, has shown promise in reducing NOX emissions and reducing maximum heat release rate for a hydrogen DI engine [6, 17]. An explanation for the fit of the model could be that the NO formation is a function of time and temperature. Higher loads will require more fuel and thus a larger total heat release, while a short burn duration will lead to much higher peak temperatures.

SOI sweep To capture the effects of injection timing in greater detail, especially closer to IVC, a range of injection timings from -310 °ATDC to -130 °aTDC was used at a load of 9 bar IMEP and a speed of 2000 rpm. As the injection of hydrogen will displace a significant volume of charge air when the intake valves are open, the intake pressure could be reduced to maintain the lambda at 2 as the SOI moved closer to TDC as shown in Figure 10. The exhaust back pressure was adjusted to match the intake pressure, similar to the previous rounds of experiments. Especially for injection timings that are late enough that part of the injection will take place after the intake valve is closed, the intake pressure was reduced.

The NOX emissions also show a small increase as the SOI is delayed, as shown in Figure 10. As the average λ and load was kept constant, a possible explanation is that late SOI gives less time for mixing the air and fuel, and the resulting relatively rich zones could have a negative impact on the NOX emissions.

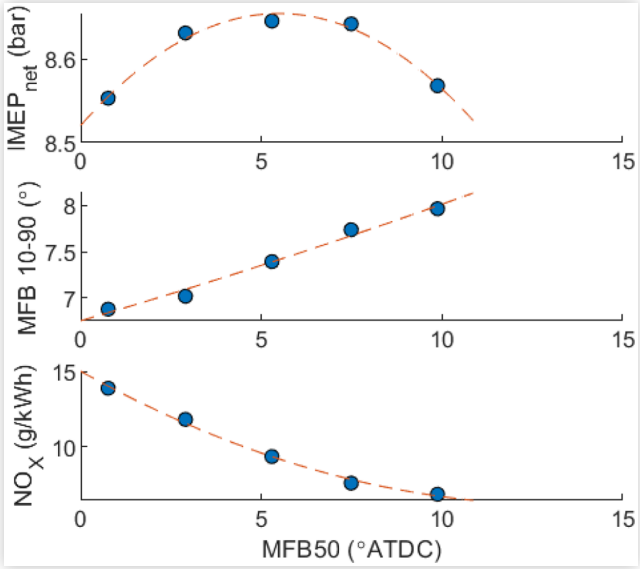
Ignition sweep There was an uncertainty whether MBT timing would still be obtained when the combustion phasing is such that the MFB50 is around 8 °aTDC, and thus all the points in the baseline map and the DoE part of the experiments were evaluated with a range of spark timings.

A second-degree polynomial was fitted to the data and used to interpolate a value for the combustion phasing that would lead to the highest IMEP$_{net}$ The behavior shows a plateau of high IMEP$_{net}$ over a range of combustion phasings between approximately 3 and 8 °aTDC through most of the operating points. Figure 11 shows the effect of combustion phasing for an example operating point where the speed was 2000 rpm, the target λ was 1.5, and the target load was 9 bar IMEP$_{net}$.

Combustion phasing also influences the NOX emissions, as well as the combustion duration. The NOX emissions appear to increase exponentially with load, while the combustion duration, defined as the time between MFB10 and MFB90, increases as the start of the combustion is delayed.

The results show that there is an increase in NOX emissions as the timing, hence the combustion phasing, is advanced. This implies that the emissions could increase drastically if the combustion phasing is advanced from e.g., MFB50

FIGURE 11 Effects of combustion phasing on net IMEP, MFB 10-90 and NO$_X$ emissions.



Downloaded from SAE International by Chalmers University of Technology, Friday, November 06, 2026

at 8 to 4 °aTDC, especially for load cases with lower A/F ratios, such as the one shown in Figure 11. The relatively flat IMEP curve shown in Figure 11 implies that spark timing should preferably be retarded rather than being advanced, for emissions benefit while keeping the efficiency similar.

NO_2 to NO ratio According to the results from the map and DoE experiments, a hydrogen SI engine will need an exhaust aftertreatment system to comply with legislation regarding NOx emissions, as the proposed limits for the hot cycle is reduced to 90 mg/kWh, which the engine exceeds for most loads over 6 bar $IMEP_{net}$, as shown in Figure 6. The fastest and most efficient route in a conventional diesel engine SCR system is as the fast reaction path, which requires a 1:1 ration of NO to NO2 [18], however the results from a combination of the data points from the DoE and mapping experiments, including the variations in spark timing, show that the ratio skews heavily towards NO at NOX levels as low as 0.1 g/kWh. as shown in Figure 12. This would imply that the DOC that can normally be used to maintain a 1:1 ratio of NO to NO_2 will be able to serve that purpose for a hydrogen SI engine as well.

Hydrocarbons

The total hydrocarbon emissions of the engine, reported as propane equivalent, from the FID for the load points run in the engine mapping part of the experiments are shown in Figure 13.

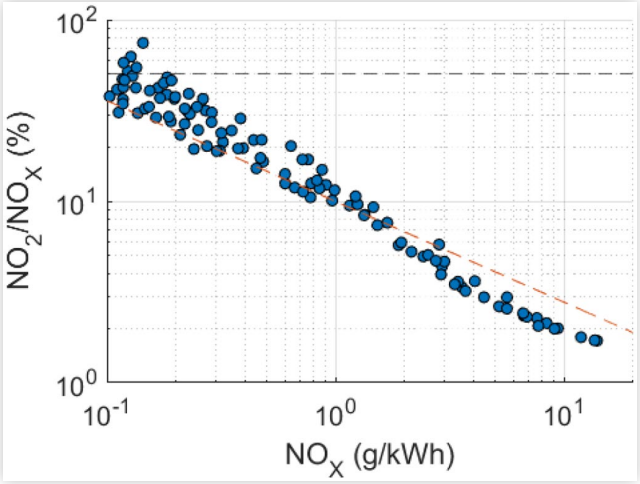
The results show that the indicated hydrocarbon emissions increase with an increasing engine speed, and that they are at their highest at low loads.

Particle Emissions

The particle emissions of the engine were measured for all data points. However, the significant variability of the measurement results made any detailed analysis of trends regarding factors such as load, speed, ignition timing, and injection timing difficult to perform with sufficient accuracy. However, a strong trend of emissions decreasing with load was observed regardless of other engine parameter variations. Figure 14 shows the results for all load points in the DoE and mapping experiments. The outliers marked in red show the variations, especially at $IMEP_{net}$ of 6 bar, which was the most frequently operated load.

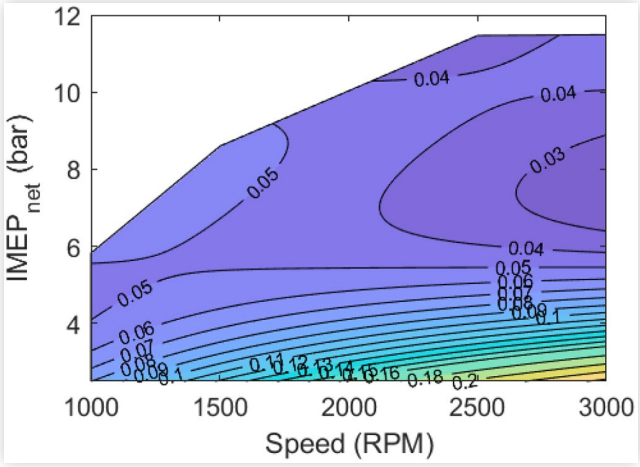
The emissions at 4.5 bar and higher, are typically only a fraction (about 1%) of the emissions at a load of 2.5 bar IMEP net. Combustion of pure hydrogen should not produce any particles and it has been previously indicated that particle

FIGURE 12 log-log plot of NO_2 as % of total NO_X emissions vs total indicated NO_X emissions (g/kWh). The horizontal dashed line corresponds to a 1/1 ratio of NO and NO_2.



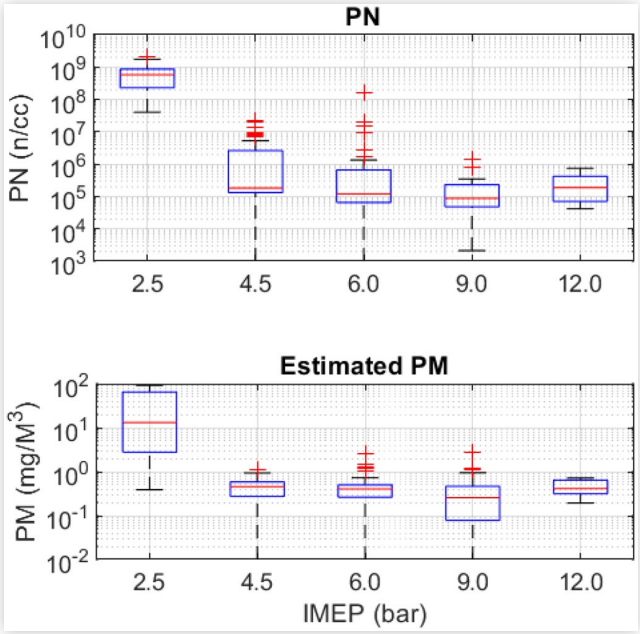
© The Author(s)

FIGURE 13 Indicated specific hydrocarbon emissions (g/kWh).



© The Author(s)

FIGURE 14 Summary of particle emissions as a function of engine load. Particle mass was estimated assuming that particles were spherical with a density of 1000 kg/m3.



© The Author(s)

Downloaded from SAE International by Chalmers University of Technology, Friday, November 06, 2026

emissions from a hydrogen engine are caused by partial combustion of engine oil [5, 12, 13].

ICP analysis of particles sampled on filters confirm that the particulates contain compounds from the engine oil, as they contain trace metals that are not present in the fuel or intake air, see Table 3. The iron content in the particles could be from the engine cylinder liner, while some other metals such as cadmium and zinc are most likely from oil additives.

While the ICP analysis shows that particle matter at least partly contains oil-based components, the results from the Sunset analysis showed that not only where the particles most likely oil, but most of the oil was unburned, and most of the matter collected on the filters were organic carbon compounds. The proportion of elemental carbon in relation to the organic carbon was found to be extremely low. The results show that the FID signal in the measurement instrument bottoms out at low temperature, see Figure 15.

The saturation of the instrument at low temperatures in the absence of oxygen suggests that the filters contained very high content of more volatile organic hydrocarbons. While the latest peak, after oxygen and methane are introduced is high, the short time where the signal is high means that the total elemental carbon content is low. The ratio of organic to elemental caron is thus very high. The saturation at low temperatures occurred for both samples, meaning that the actual ratio of elemental carbon to organic carbon may be even lower. A possible solution would be to sample less particles on the filter, but in doing so the elemental carbon levels may go under the detection limit of the instrument. A summary of the results is given in Table 4.

Since the instrument bottomed out on the organic carbon, detailed comments on the ratio of organic carbon to elemental carbon are not possible, however the results show that for both samples the ratio is less than 0.1% elemental carbon to organic carbon, meaning almost all the measured particle emissions were in fact unburned oil droplets.

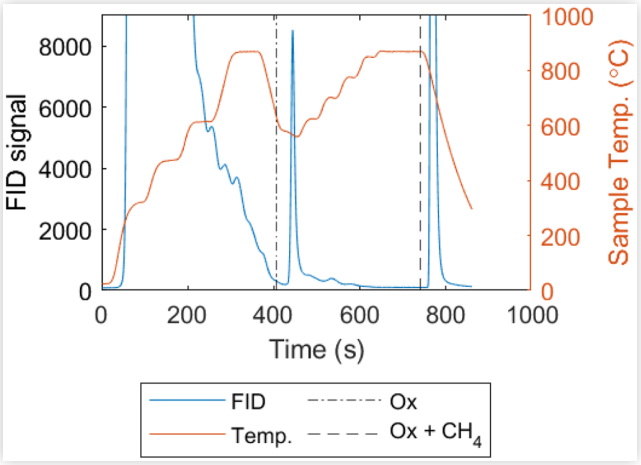
A possible explanation for the increased particle emissions at low load is that at low intake pressure, the pressure difference between the intake and the camshaft compartment of the cylinder head may push oil past the valve stem seals and guides in the intake ports. The corresponding low cylinder pressure during the intake stroke may also contribute to increased blow-back from the crankcase (at atmospheric pressure) past the piston rings. Both these mechanisms could deposit engine oil in the cylinder and combustion chamber and contribute to higher particle emissions. Since the particle emissions were found to be oil droplets, the FID results should give an indication for the particle emissions. Figure 16 shows the hydrocarbon emissions (dots) for the points included in

TABLE 3 ICP results for different estimated filter particle loading, including an empty reference filter (0).

Loading (mg)	0.7	2.1	5.9	0
Aluminum (µg)	2.98	2.46	2.42	2.98
Molybdenum (µg)	0.0273	0.11	0.201	0.00398
Zinc (µg)	1.72	6.76	10.6	<0.5
Boron (µg)	<1	<1	<1	<1
Calcium (µg)	8.39	24.2	41.1	3.52
Copper (µg)	0.0922	0.216	0.238	0.0252
Iron (µg)	0.21	0.8	1.73	<0.2
Magnesium (µg)	0.77	0.641	0.642	0.7
Phosphorus (µg)	5.32	11.6	18.3	3.3
Potassium (µg)	<50	<50	<50	<50
Silicon (µg)	<20	<20	<20	<20
Sodium (µg)	<5	<5	<5	<5
Sulfur (µg)	5.86	12.5	17.2	<2

© The Author(s)

FIGURE 15 FID signal in arbitrary units (blue) and temperature (red) over time from the Sunset OC/EC analysis of the first sample. The vertical lines indicate where first oxygen, and later oxygen and methane are introduced. The figure shows how the FID signal saturates at low temperatures.



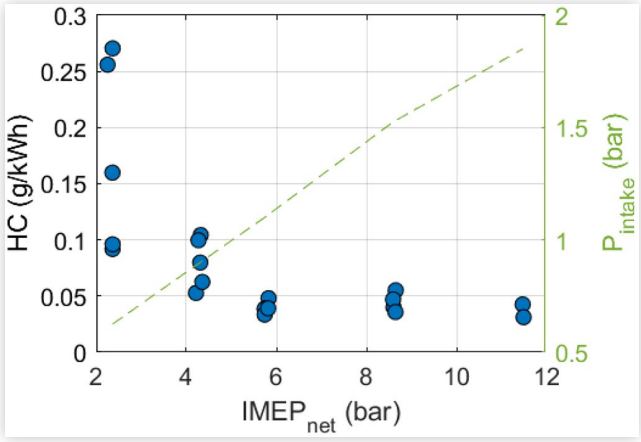
© The Author(s)

TABLE 4 Summary of Sunset OC/EC analysis. The level of elemental carbon is close to the detection limit.

Sample Time (minutes)	OC (µg/cm²)	Total OC on filter (µg)	EC (µg/cm²)	Total EC on filter (µg)
30	392	3400	0.36	3
10	477	4100	0.25	2

© The Author(s)

FIGURE 16 Indicated specific THC emissions in ppm. As the intake pressure (dashed line) decreases at low engine loads, emissions of hydrocarbons (dots) increase.



© The Author(s)

Downloaded from SAE International by Chalmers University of Technology, Friday, November 06, 2026

the engine mapping experiments as a function of engine load. The intake pressure (dashed line) is shown only for 2500 rpm as the variations of the required intake pressure due to engine speed are relatively small. High THC emissions at low intake pressures seem to confirm the theory, as the intake pressure is below atmospheric at these points.

The results are contradictory to the findings of Li et.al [19], who stated that a hydrogen engine that runs at constant intake pressure at increased load consumed more oil as load and equivalence ratio increased, which the Author(s) attributed to the reduced quenching distance. While the low quenching distance seems to be a key factor that explains the high amount of oil interaction in a hydrogen engine, it does not explain the results of the current experiments, as the quenching distance should not increase with load, as higher loads would increase both the charge density and cylinder temperature.

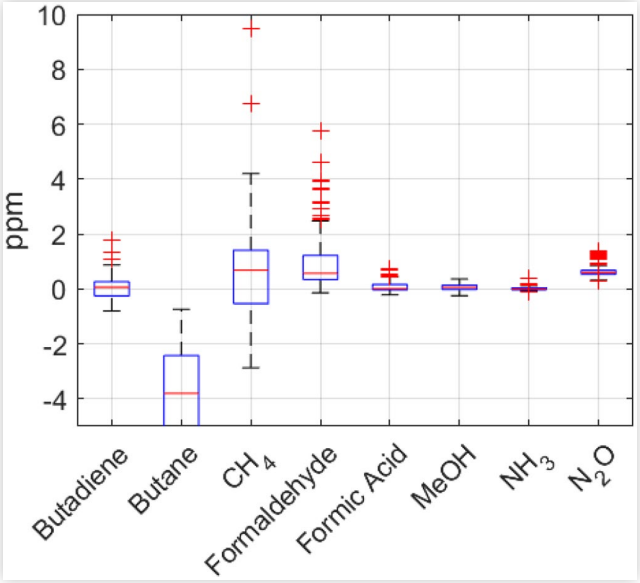
The current investigation suggests that at low load, throttled operation of a hydrogen fueled SI engine should be minimized. Measures that reduce the need for throttling the engine could be early SOI, at open intake valves, to take advantage of the volume occupied by the hydrogen, combined with high A/F ratios to increase the total charge volume and intake pressure required for a given load. Once the intake pressure exceeds atmospheric pressure or crank-case pressure, the strategy does not seem to matter for particle emissions and can be optimized for low NOX and high efficiency.

Unregulated Emissions

The emissions of some of the components measured with the FTIR system is presented in Figure 17. Most of the emissions measured were low, with N2O the only component where a trend between measurement points could be observed. Many of the hydrocarbon species measured individually with the FTIR shows a relatively large spread between measurements, with averages close to zero. There is not enough data to draw conclusions about what could be influencing the levels, but that the emissions are insignificantly low can be confirmed.

The negative values measured for the butane emissions are most likely caused by interference with other species in the exhaust, as the emissions of hydrocarbon species are low and the infrared emission spectra of butane is wide. It is thus hard to avoid interference with other species in the exhaust.

FIGURE 17 Previously unregulated emissions in ppm. The box indicates data between 25th and 75th percentile, while the whiskers indicate the most extreme values not considered outliers. The red crosses indicate the outliers.



Conclusions

This paper aimed to investigate the effects of operation parameters such as load, speed, injection timing, air- fuel-ratio and ignition timing on the emissions and performance of a direct injection spark ignition internal combustion engine operated on pure hydrogen. Three experimental campaigns are included in this paper. The first, an investigation on the effects of speed and load at a constant A/F ratio. The second campaign was a design of experiments aimed at investigating the combined effects of load, A/F and start of injection. For both campaigns several spark timings were used. Lastly, sweeps of injection timing and ignition timing at constant load and speed were performed. General findings indicate that a hydrogen combustion engine can be operated in modes that produce very low emissions, but that an exhaust aftertreatment system will be required to consistently reach emission limits, especially considering particle emissions at part load. Indicated efficiencies reaching higher than 40% were possible for a large range of loads and operating conditions.

Further conclusions:

- NOX emissions are low provided that the engine is operated at high A/F ratios. The emissions increase exponentially with lowered A/F ratio and early spark timing and can exceed 10 g/kWh at $\lambda = 1.5$.
- While the NOX emissions vary with λ, load, combustion phasing and start of injection, NOx emissions can be predicted using only burn duration from MFB10 to MFB90 and IMEPnet.
- Spark timing influences the IMEP of the engine and shows a maximum when MFB50 is between 4 and 8° aTDC, while the burn duration from 10% to 90% MFB increases as the combustion phasing is delayed. The shorter burn duration at early ignition timings is associated with an exponential increase in NOX emissions.
- Particle numbers increase exponentially with low load and is most likely caused by oil ingression due to low intake pressure and measured particles reach numbers as high as 1e9 n/cc, corresponding to 2e15 n/kWh. Variability between measurements is significant, but the trend of decreasing emissions with increasing load is very strong for all engine speeds tested.

© The Author(s)

Downloaded from SAE International by Chalmers University of Technology, Friday, November 06, 2026

- The particles emitted are of small size, with most common sizes in the 10 to 30 nm range for most loads and speed combinations.
- Analysis of particles collected on filters show very low soot content and high content of organic carbon compared to diesel particles. Less than 0.1 % of the carbon was elemental carbon (soot), which means that most of the measured particles were organic carbon compounds and thus oil droplets.
- Hydrocarbon emissions were present in the exhaust at concentrations around the measurement limit of the FID used and follows the same trend of increasing emissions at low intake pressure as the particle emissions.
- At low load, throttled operation of a hydrogen fueled SI engine should be minimized to avoid particle emissions. Measures that reduce the need for throttling the engine could be early hydrogen injection, during open intake valves, where higher intake pressure is needed to maintain a required volumetric efficiency. Once the intake pressure exceeds atmospheric pressure or crank-case pressure, the strategy does not seem to matter for particle emissions and can be optimized for low NOX and high efficiency
- ICP analysis found metal traces in the particulate matter that was sampled consistent with engine oil, further strengthening the hypothesis that the particles measured were from the engine oil.
- Emissions of previously unregulated species were measured by FTIR. The engine was confirmed to produce trace amounts of hydrocarbons, as well as around 1 ppm of formaldehyde and N2O.

Acknowledgements

The Author(s) would like to thank Scania, Volvo Trucks and Johnson Matthey, FFI and the Swedish Energy Agency for their support.

We would also thank Tobias Storsjö at the School of Public Health and Community Medicine, Gothenburg University, Gothenburg, Sweden, for his help with the Sunset OC/EC analysis.

Finally, we would also like to thank Timothy Benham, Anders Mattsson and Alf Magnusson for their support with the test equipment and facilities.

References

1. Dawood, F., Anda, M., and Shafiullah, G.M., "Hydrogen Production for Energy: An Overview," *International Journal of Hydrogen Energy* 45, no. 7 (2020): 3847-3869, doi:https://doi.org/10.1016/j.ijhydene.2019.12.059.
2. Yue, M. et al., "Hydrogen Energy Systems: A Critical Review of Technologies, Applications, Trends and Challenges," *Renewable and Sustainable Energy Reviews* 146 (2021): 111180, doi:https://doi.org/10.1016/j.rser.2021.111180.
3. Verhelst, S., "Recent Progress in the Use of Hydrogen as a Fuel for Internal Combustion Engines," *International Journal of Hydrogen Energy* 39, no. 2 (2014): 1071-1085, doi:https://doi.org/10.1016/j.ijhydene.2013.10.102.
4. Oikawa, M. et al., "Attainment of High Thermal Efficiency and Near-zero Emissions by Optimizing Injected Spray Configuration in Direct Injection Hydrogen Engines," SAE Technical Paper 2019-01-2306 (2019), doi:https://doi.org/10.4271/2019-01-2306.
5. Thawko, A. et al., "Particle Emissions of Direct Injection Internal Combustion Engine Fed with a Hydrogen-Rich Reformate," *International Journal of Hydrogen Energy* 44, no. 52 (2019): 28342-28356, doi:https://doi.org/10.1016/j.ijhydene.2019.09.062.
6. Nande, A.M., Wallner, T., and Naber, J., "Influence of Water Injection on Performance and Emissions of a Direct-Injection Hydrogen Research Engine," SAE Technical Paper 2008-01-2377 (2008), doi:https://doi.org/10.4271/2008-01-2377.
7. Yip, H.L. et al., "A Review of Hydrogen Direct Injection for Internal Combustion Engines: Towards Carbon-Free Combustion," *Applied Sciences* 9 (2019): 4842, doi:https://doi.org/10.3390/app9224842.
8. Oh, S. et al., "Analysis of the Exhaust Hydrogen Characteristics of High-Compression Ratio, Ultra-Lean, Hydrogen Spark-Ignition Engine Using Advanced Regression Algorithms," *Applied Thermal Engineering* (2022): 215, doi:https://doi.org/10.1016/j.applthermaleng.2022.119036.
9. Bekdemir, C., Doosje, E., and Seykens, X., "H2-ICE Technology Options of the Present and the Near Future," SAE Technical Paper 2022-01-0472 (2022), doi:https://doi.org/10.4271/2022-01-0472.
10. De Bellis, V. et al., "Experimental and 0D Numerical Investigation of Ultra-Lean Combustion Concept to Improve the Efficiency of SI Engine," SAE Technical Paper 2021-01-0384 (2021), doi:https://doi.org/10.4271/2021-01-0384.
11. "COM(2022) 586 ANNEX - Annex to the COM(2022) 586 Proposal for a Regulation," Internal Market, Industry, Entrepreneurship and SMEs/Publications, 2023.
12. Maier, A., Dreizler, A., and Rottengruber, H., "Fuel-Independent Particulate Emissions in an SIDI Engine," *SAE Int. J. Engines* 8, no. 3 (2015): 1334-1341, doi:https://doi.org/10.4271/2015-01-1081.
13. Thawko, A. et al., "Effect of Lubricant Formulation on Characteristics of Particle Emission from Engine Fed with a Hydrogen-Rich Fuel," SAE Technical Paper 2020-01-2200 (2020), doi:https://doi.org/10.4271/2020-01-2200.
14. Melaika, M., Herbillon, G., and Dahlander, P., "Spark Ignition Engine Performance, Standard Emissions and Particulates Using GDI, PFI-CNG and DI-CNG systems," *Fuel* 293 (2021): 120454, doi:https://doi.org/10.1016/j.fuel.2021.120454.
15. "Regulation (EC) No 595/2009 of the European Parliament and of the Council of 18 June 2009 on type-Approval of Motor Vehicles and Engines with Respect to Emissions from Heavy Duty Vehicles (Euro VI) and Amending Regulation (EC) No 715/2007 and Directive 20. EUR-Lex," 2023.

Downloaded from SAE International by Chalmers University of Technology, Friday, November 06, 2026

16. "Directorate-General for Internal Market, I., Entrepreneurship and SMEs COM(2022) 586 ANNEX - Annex to the COM(2022) 586 Proposal for a Regulation," 2023.
17. Younkins, M., Wooldridge, M.S., and Boyer, B.A., "Port Injection of Water into a DI Hydrogen Engine," SAE Technical Paper 2015-01-0861 (2015), doi:https://doi.org/10.4271/2015-01-0861.
18. "Selective Catalytic Reduction," 2023.
19. Li, H., Karim, G.A., and Sohrabi, A., "Examination of the Oil Combustion in a S.I. Hydrogen Engine," SAE Technical Paper 2004-01-2916 (2004), doi:https://doi.org/10.4271/2004-01-2916.

Abbreviations

A/F - Air Fuel
DI - Direct Injection
DoE - Design of Experiments
EVC - Exhaust valve Closing
EVO - Exhaust Valve Opening
FTIR - Fourier-Transform Infrared Spectroscopy
ICP - Inductively Coupled Plasma
IMEP - Indicated Mean Effective Pressure
$IMEP_{net}$ - Net Indicated Mean Effective Pressure
IVC - Intake Valve Closing
IVO - Intake Valve Opening
MBT - Maximum Brake Torque
MFB - Mass Fraction Burned
MFB10 - Mass Fraction Burned = 10%
MFB50 - Mass Fraction Burned = 50%
MFB90 - Mass Fraction Burned = 90%
NO - Nitric Oxide
NO_X - Nitrogen Oxides
OC/EC - Organic Carbon Elemental Carbon
PFI - Port Fuel Injection
PM - Particle Mass
PN - Particle Number
THC - Total Hydrocarbon

© 2023 The Author(s); Published by SAE International. This Open Access article is published under the terms of the Creative Commons Attribution License (http://creativecommons.org/licenses/by/4.0/), which permits distribution, and reproduction in any medium, provided that the original author(s) and the source are credited.

Positions and opinions advanced in this work are those of the author(s) and not necessarily those of SAE International. Responsibility for the content of the work lies solely with the author(s).

e-ISSN 2641-9645